Research Article

Check for updates

Stiffness-tunable and shape-locking soft actuators based on 3D-printed hybrid multi-materials

Jian Jiao[1], Yuan Guo[2], Qianqian Tong[1], Shengkai Liu[3,*], Pengfei Qiu[4], Tao Mei[1], Dangxiao Wang[1,2,*]

[1]Peng Cheng Laboratory, Shenzhen 518055, Guangdong, China.
[2]State Key Lab of Virtual Reality Technology and Systems and Beijing Advanced Innovation Center for Biomedical Engineering, Beihang University, Beijing 100191, China.
[3]School of Mechanical Engineering, Beijing Institute of Technology, Beijing 100081, China.
[4]State Key Laboratory of Coordination Chemistry, School of Chemistry and Chemical Engineering, Collaborative Innovation Center of Advanced Microstructures, Nanjing University, Nanjing 210023, Jiangsu, China.

*Correspondence to: Dr. Shengkai Liu, School of Mechanical Engineering, Beijing Institute of Technology, No. 5 Zhongguancun South Street, Beijing 100081, China. E-mail: liushengkai@bit.edu.cn; Prof. Dangxiao Wang, State Key Lab of Virtual Reality Technology and Systems and Beijing Advanced Innovation Center for Biomedical Engineering, Beihang University, No. 37 Xueyuan, Beijing 100191, China. E-mail: hapticwang@buaa.edu.cn

Abstract

Soft actuators have been receiving tremendous attention as a result of their excellent adaptability to the environment. However, due to their inherently low stiffness, soft actuators are difficult to adapt to high-load tasks. Despite previous efforts in developing stiffness-tunable actuators by utilizing variable stiffness materials, they still suffer from limitations, including relatively low load and locking capacity to grasp weights and difficulties regarding their fabrication with complex structures. This work reports a novel stiffness-tunable and shape-locking soft (Tri-S) actuator using hybrid multi-material 3D printing. The Tri-S actuator consists of polylactic acid, thermoplastic polyurethane and a flexible carbon fiber heating wire. Its stiffness can be effectively tuned by Joule heating. A soft robotic gripper equipped with three Tri-S actuators demonstrates their stiffness-tunable and shape-locking capability by grasping and holding objects of various shapes and weights. The gripper can grasp weights up to 2.2 kg with an external driving force by tuning the stiffness and hold weights up to 310 g depending on its own shape locking without an external driving power source.

Keywords: Stiffness tunable, shape locking, hybrid multi-materials, 3D printing, soft actuators

INTRODUCTION

In recent years, with the booming development of soft robots, soft actuators have shown tremendous potential[1-4]. Such actuators have better compliance and adaptability to the environment because of their softness[5-8]. They can provide high flexible locomotion and greatly reduce the contact impact, which can effectively improve the security of interaction[9-11]. Due to these advantages, soft actuators have significant potential prospects[12-14]. Our group has developed a series of soft actuators[15-17]. Owing to their inherent low stiffness, however, they could not easily meet the requirements of high-load tasks. Therefore, it is necessary to improve the load capacity of soft robots by modulating the stiffness of soft actuators[18-20]. Regarding the stiffness modulation of soft actuators, many previous works have been carried out, including variable stiffness mechanisms and stiffness materials[21-24].

As typically variable stiffness approaches, jamming mechanisms can tune the stiffness of soft actuators by controlling the shear stress produced by the particles or layers within elastic membranes due to the application of a vacuum[25-27]. Li *et al.* patched a silicone rubber soft actuator and a pack of particles to form an integral gripping finger[28]. The soft actuator exerted pressure on the particle pack through its own inflation, resulting in the particles jamming, thereby increasing the stiffness of the finger. Kim *et al.* proposed a layer vacuum jamming method, which employed the friction between layers to tune the stiffness of the mechanism[29]. Different from vacuum-based jamming, Jiang *et al.* designed a chain-like jamming mechanism, which was able to achieve a large range of stiffness modulation instantly by pulling a thread[30]. However, these jamming mechanisms are relatively complex and also require additional power source supplies for changing stiffness, such as pneumatic pressure sources, electric motors, and so on.

Many materials, such as low glass transition polymers and low melting point alloys can tune their stiffness by changing the temperature under heating stimulation[31-36]. This outstanding advantage has attracted the interest of many researchers. Zhang *et al.* presented a stiffness-tunable soft actuator fabricated by hybrid multi-material three-dimensional (3D) printing with shape memory polymer layers[37]. They equipped a stiffness-tunable robotic gripper with the actuators, which was able to grasp a 1.5 kg dumbbell. Schubert *et al.* embedded a low melting point alloy into polydimethylsiloxane to form a stiffness-tunable soft actuator whose stiffness could be effectively tuned by changing the temperature[38]. Taghavi *et al.* proposed a 3D-printed variable stiffness structure through the combination of polylactic acid (PLA) and conductive graphene PLA[23]. The stiffness of the structure could be controlled by Joule heating. By using a 3D-printed conductive polylactic acid (CPLA) material, Al-Rubaiai *et al.* proposed a variable stiffness actuator[39]. They embedded the CPLA material in a silicone pneumatic soft actuator to realize the stiffness modulation by Joule heating, which could withstand a maximum payload of 800 g. The shape-locking capability can keep the holding tasks by fixing soft actuators into a temporary shape in the absence of an external force, thereby effectively saving the energy output of the driving power source. Ze *et al.* compounded magnetic particles into a shape memory polymer to form a shape-programmable soft material and manufactured a shape-locking gripper using the material, which could lock a ball with a weight of 23 g[24]. A shape-lockable gripper composed of two soft pneumatic actuators with a CPLA material was developed by Al-Rubaiai *et al.*, which was able to lock a lightweight plushy mini football[39]. However, the mechanical properties of CPLA materials (including graphene PLA) can become worse, owing to the doping of conductive substances (such as graphene, carbon nanotubes, silver nanowires, and so on). An obvious feature is an increase in their brittleness in natural circumstances.

Despite previous efforts to develop stiffness-tunable soft actuators by adopting variable stiffness materials, the current components generally suffer from several limitations, including relatively low load and locking levels and difficulties regarding their fabrication with complex structures. Hence, there is still an

opportunity for easy-to-fabricate, high-loading and shape-lockable actuators. In this study, we present a novel stiffness-tunable and shape-locking soft (Tri-S) actuator fabricated using thermoplastic polyurethane (TPU) and PLA materials through 3D-printed hybrid multi-material manufacturing technology. By supplying electricity to the flexible carbon fiber (CF) heating wire embedded in the PLA, the stiffness of the Tri-S actuator can be conveniently tuned by Joule heating. We equip a soft robotic gripper with three Tri-S actuators. Due to the capability of the actuators to the tunable stiffness, it cannot only safely grasp fragile objects (such as an egg) under low stiffness, but also adapt to heavy load tasks (such as a metal bar) under high stiffness. The soft robotic gripper is able to grasp weights up to 2.2 kg with an external driving force and hold weights up to 310 g depending on its own shape locking without an external driving power source, which could be difficult for existing soft grippers. The Tri-S actuator cannot only bear a large load by the stiffness-tunable function but can also save the driving energy supply in holding tasks by the shape-locking function.

The main contributions of our work can be summarized as follows:

(1) Through the combination of a PLA material with a low glass transition temperature and a TPU material with high elasticity, the proposed Tri-S actuator possesses the abilities of tunable stiffness and shape locking. The actuator is able to withstand and lock high loads, which could be difficult to achieve for existing soft actuators.

(2) Via hybrid multi-material 3D printing, the Tri-S actuators can be integrally fabricated through the switching of multiple nozzles with different materials, which are easy to fabricate, address the difficulties in microfeature fabrication, such as microchannels and embedded microstructures, and have dramatically reduced fabrication costs.

MATERIALS AND IMPLEMENTATION
Design and fabrication
We designed a tendon-driven soft robotic actuator, as shown in Figure 1. The 3D models of the soft robotic actuator were first designed with computer aided design. Figure 1A shows the composition of the Tri-S actuator, including an elastomeric body of TPU [White (1755), Ultimaker, Netherlands] with an elastic modulus of 78.7 MPa, a tunable stiffness slice of PLA [Magenta (1617), Ultimaker, Netherlands], a flexible CF heating wire and a driving tendon. Considering that TPU is a type of highly elastic soft material, we employed it as the main body material of the Tri-S actuator. It can endow the Tri-S actuator with an elastic recovery ability. Under the combined effects of PLA and TPU, the Tri-S actuator not only possesses tunable stiffness but also has the capacity for shape recovery.

The main frame of the Tri-S actuator includes a TPU body and an embedded PLA slice. Some axial holes were uniformly distributed in the inner of the PLA slice. Through these holes, the CF heating wire was assembled into the PLA slice and generated uniform Joule heating. A driving tendon was inserted into the tendon holes to control the Tri-S actuator bending. When the stiffness of the Tri-S actuator needs to be adjusted, a direct current power is applied at both ends of the CF heating wire to produce Joule heating. The PLA began to soften as the temperature rose after electric heating. The stiffness of the Tri-S actuator can be effectively tuned by controlling the input voltage applied at both ends of the CF heating wire.

The stiffness-tunable structure in the Tri-S actuator mainly includes a PLA slice and a flexible CF heating wire. PLA is a type of low glass transition temperature material with a relatively narrow controllable temperature range and exhibits high rigidness at low temperature and good softness at high temperature. In
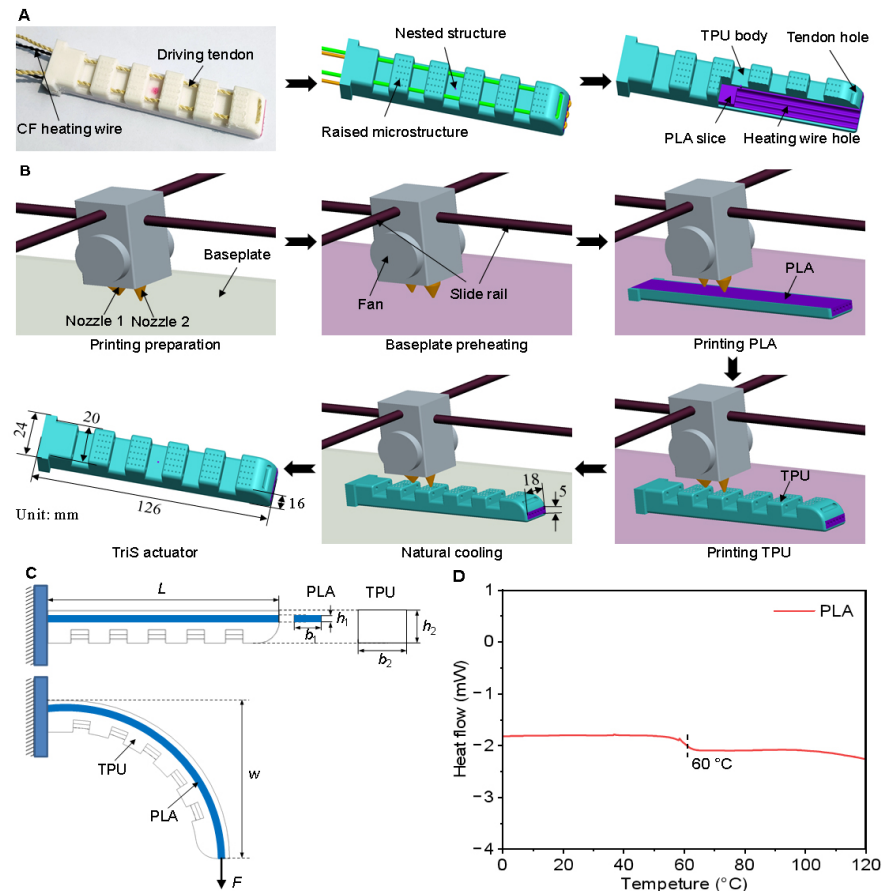
Figure 1. Design and fabrication of a Tri-S actuator. (A) Illustration of Tri-S actuator composition. (B) Tri-S actuator manufacturing processes by 3D-printed hybrid multi-material technology. (C) Description of Tri-S actuator with rectangular cross sections. (D) Test of Tg for PLA by differential scanning calorimetry analysis. PLA: polylactic acid; TPU: thermoplastic polyurethane.

this regard, the stiffness of the PLA slice structure can be tuned by controlling the temperature. Moreover, its stiffness can be tuned by a relatively small amount of heat. Herein, we employed PLA as the tunable stiffness material of the Tri-S actuator. In order to produce significant Joule heating, the flexible CF heating wire was embedded into the inner part of the PLA slice structure in the Tri-S actuator.

In view of the difficulties in machining microstructures, such as raised microstructures, nested structures and heating wire and tendon holes, the Tri-S actuator body was integrated via a hybrid multi-material 3D printing method using a commercial double-nozzle fused deposition modeling 3D printer (S5, Ultimaker, Netherlands). As shown in Figure 1B, the PLA filament was loaded in nozzle 1 of the 3D printer and the TPU filament was loaded in nozzle 2. In the 3D printing process, the two nozzles are switched to each other according to the material requirements of the different parts of the Tri-S actuator. The printing temperature and velocity were set to 230 °C and 35 mm/s for the TPU and 200 °C and 70 mm/s for the PLA, respectively. After printing, the Tri-S actuator was naturally cooled to room temperature to prevent deformation and then removed from the 3D printer. We realize the easy-to-fabricate Tri-S actuator body using hybrid multi-material 3D printing. A CF heating wire was installed into the heating wire holes in the PLA of the Tri-S actuator. We assembled a Kevlar thread into the tendon holes in the TPU of the Tri-S actuator as the driving tendon.

Modeling analysis

To analyze the impact of the PLA and TPU parameters on the performance of the Tri-S actuator, we establish a theoretical model for describing their relationship. As can be seen in Figure 1C, a deflection will be generated when an external force F is applied to the distal end of the Tri-S actuator. Considering Euler-Bernoulli beam theory[30], the bending stiffness k of the Tri-S actuator can be estimated as

$$k = \frac{F}{w} = \frac{3EI}{L^3} \tag{1}$$

where w is the deflection caused by the bending force, E refers to the elastic modulus and I denotes the moment of inertia. For a Tri-S actuator with a length L, we can deduce that the bending stiffness k depends completely on the moment of the inertia I. The moment of inertia can be given as

$$I = \frac{bh^3}{12} \tag{2}$$

where b is the width of PLA. According to the assumptions already mentioned, h is the thickness.

By substituting Equation (2) into Equation (1), a relationship between the bending stiffness and the dimensions of the actuator can be obtained as

$$k = \frac{Ebh^3}{4L^3} \tag{3}$$

According to Equation (3), we can obviously find that the bending stiffness k is proportional to the width b and the thickness h, and inversely proportional to the length L. Therefore, the greater the thickness, the larger the bending stiffness.

When an external force F is applied to the distal end of the Tri-S actuator, the resistance forces produced by PLA and TPU are F_1 and F_2, respectively. The sum of the resistance forces is equal to the external force, that is

$$F = F_1 + F_2 \tag{4}$$

From Equation (1), the total resistance force can be calculated as

$$F = F_1 + F_2 = k_1 w + k_2 w = (k_1 + k_2)w \tag{5}$$

where k_1 and k_2 denote the bending stiffness of PLA and TPU, respectively.

According to Equation (3), the bending stiffness can be expressed as

$$k_1 = \frac{E_1 b_1 h_1^3}{4L^3}, \quad k_2 = \frac{E_2 b_2 h_2^3}{4L^3} \tag{6}$$

where E_1 and E_2 are the elastic moduli of PLA and TPU, b_1 and b_2 are the widths of PLA and TPU and h_1 and h_2 are the thicknesses of PLA and TPU, respectively.

By substituting Equation (6) into Equation (5), we obtain the following relationship

$$F = (k_1 + k_2)w = \left(\frac{E_1 b_1 h_1^3}{4L^3} + \frac{E_2 b_2 h_2^3}{4L^3}\right)w \tag{7}$$

Thus, according to Equation (8), the total bending stiffness of the Tri-S actuator can be obtained as

$$k = k_1 + k_2 = \frac{E_1 b_1 h_1^3}{4L^3} + \frac{E_2 b_2 h_2^3}{4L^3} \tag{8}$$

For the tunable stiffness, both PLA and TPU create resistance to external load. From Equation (8), we find that the stiffness of the Tri-S actuator increases with increasing PLA thickness when the other conditions remain unchanged. Nevertheless, PLA becomes soft and its elastic modulus decreases when Joule heating is supplied and the stiffness of the actuator reduces. Therefore, the stiffness of the Tri-S actuator can be effectively tuned by Joule heating.

For the shape recovery, there is no external load in this situation. However, the resistant force produced by PLA reacts with the restoring force of TPU at that time, which prevents the shape recovery of TPU. According to Equation (8), the stiffness of TPU increases with its increasing thickness when the other conditions remain unchanged. As a result, the elastic recovery force will increase accordingly. Therefore, the shape recovery percentage of the Tri-S actuator increases when the TPU thickness increases. Furthermore, the elastic modulus of PLA reduces while being heated, but it cannot reduce infinitely, i.e., the resistance force of PLA always exists. This indicates that the shape recovery percentage of the Tri-S actuator cannot reach 100%.

Hence, the bending stiffness not only determines the load capacity of the actuator but also determines the shape recovery ability. The greater the PLA thickness, the greater the stiffness of the Tri-S actuator. Relatively, the greater the TPU thickness, the greater the shape recovery percentage of the actuator.

We calculated the heating energy Q generated from the circuit of the CF heating wire via Joule's law:

$$Q = I^2 R t = \frac{U^2 t}{R} \tag{9}$$

where I is the electric current flowing through the CF heating wire, R is the resistance at both ends of the CF heating wire, t is the electrified time and U is the input voltage applied at both ends of the CF heating wire.

$$R = rl \tag{10}$$

where r is the resistance per unit length and l is the length of the CF heating wire.

By substituting Equation (10) into Equation (9), the heating energy can be rewritten as

$$Q = \frac{U^2 t}{rl} \tag{11}$$

According to the law of the conservation of energy, it is assumed that all the heat generated by the CF heating wire is used for the stiffness modulation of the PLA

$$Q = Cm\Delta T \tag{12}$$

where C is the specific-heat capacity of the stiffness-tunable PLA slice, m is the mass of the stiffness-tunable PLA slice and ΔT is the temperature variation of PLA.

According to Equations (11) and (12), the temperature variation ΔT of PLA can be calculated as

$$\Delta T = \frac{U^2 t}{rlCm} \tag{13}$$

To avoid risk during operation, the input voltage used to heat the CF heating wire should be as small as possible. From Equation (13), to keep the heating rate constant, the voltage can be reduced by reducing the resistance. For the tunable stiffness of PLA, the glass transition temperature (Tg) is a critical parameter. After Tg, its stiffness can be effectively tuned. To accurately obtain the Tg value, we performed differential scanning calorimetry. The result indicated that PLA had a Tg of ~60 °C, as shown in Figure 1D.

EXPERIMENTS AND DISCUSSION

In this section, a series of experiments were conducted to validate the performance of the Tri-S actuator, including the temperature variation rate, load capacity, tunable stiffness performance and shape recovery percentage.

Characterization of temperature variation and shape recovery

In this study, the stiffness of the Tri-S actuator is tuned by Joule heating. Here, we investigate the temperature variation process of the Tri-S actuator under four different applied voltages, namely, 14, 16, 18 and 20 V. In the experiment, a DC power supply (IT6721, ITECH, USA) was employed to feed electricity to the CF heating wire for heating the Tri-S actuator. A handheld infrared thermography (DS-2TPH10-3AUF, HIKVISION, China) was used to acquire the temperature data during the measurements. The experiment was performed in an air-conditioning room and the room temperature was set to 25 °C. Considering the safety of operation and the risk of burning materials, the applied voltage was limited to 20 V (a voltage of < 36 V is considered safe for humans) in the below experiments.
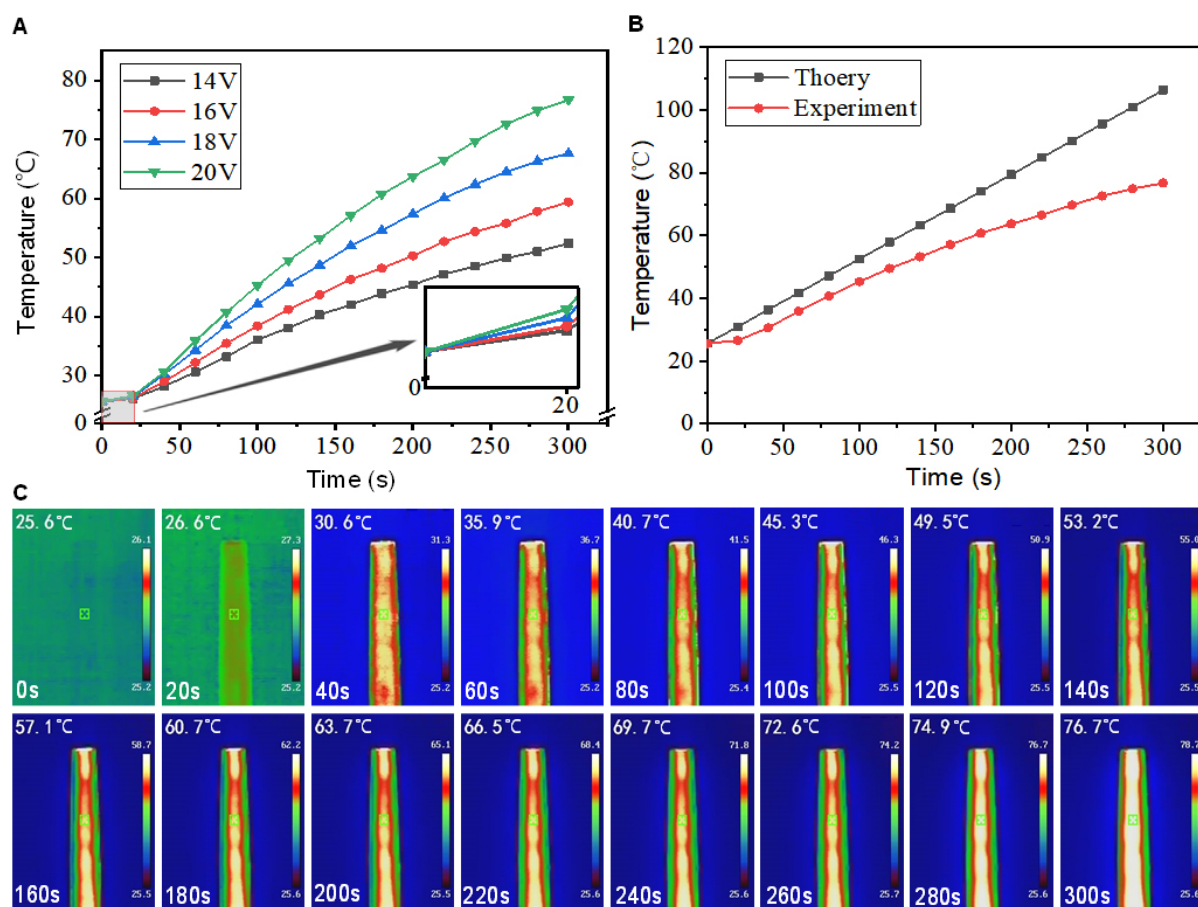
Figure 2. Characterization of temperature variation of Tri-S actuator. (A) Temperature variation of actuator as a function of electrified time. (B) Temperature comparison between theory and experiment. (C) Dynamic thermal states of Tri-S actuator at applied voltage of 20 V.

Figure 2A shows that the temperature variation of the central point of the Tri-S actuator increases with increasing time under different applied voltages. For all voltages, the temperature of the Tri-S actuator rises slowly within the first 20 s. After 20 s, the temperature begins to rise quickly with increasing time. The main reason for this is that the CF heating wire could be first preheated when the power is turned on and then heat can be conducted to the Tri-S actuator. The heating process requires time. Thus, the temperature rise emerges with minimal lag. Furthermore, the rate of the temperature rise of the Tri-S actuator is faster for the large applied voltage. The rate of temperature rise is fastest for the voltage of 20 V and the rate of the temperature rise is slowest for the voltage of 14 V. This explains that a larger applied voltage could bring higher power when the resistance is constant and generate more heat. With further increasing heating time, the temperature differences between the Tri-S actuator and the environment progressively enlarge. This will result in an increase in heat exchange between the Tri-S actuator and the environment. Therefore, the temperature rising rate of the Tri-S actuator gradually starts to slow down at the later stage. To verify the model, we conducted a comparison between the analytical and experimental results at the applied voltage of 20 V, as shown in Figure 2B. As the heating time increases, the analytical and experimental temperatures of the Tri-S actuator rise rapidly. The temperature difference between them gradually becomes larger with increasing heating time. The reason could be that the heat exchange gradually began to increase as the temperature difference between the Tri-S actuator and the surrounding environment enlarges. Some heat of the actuator is dissipated into the environment. Therefore, the temperature calculated by the model is higher than the experimental temperature.
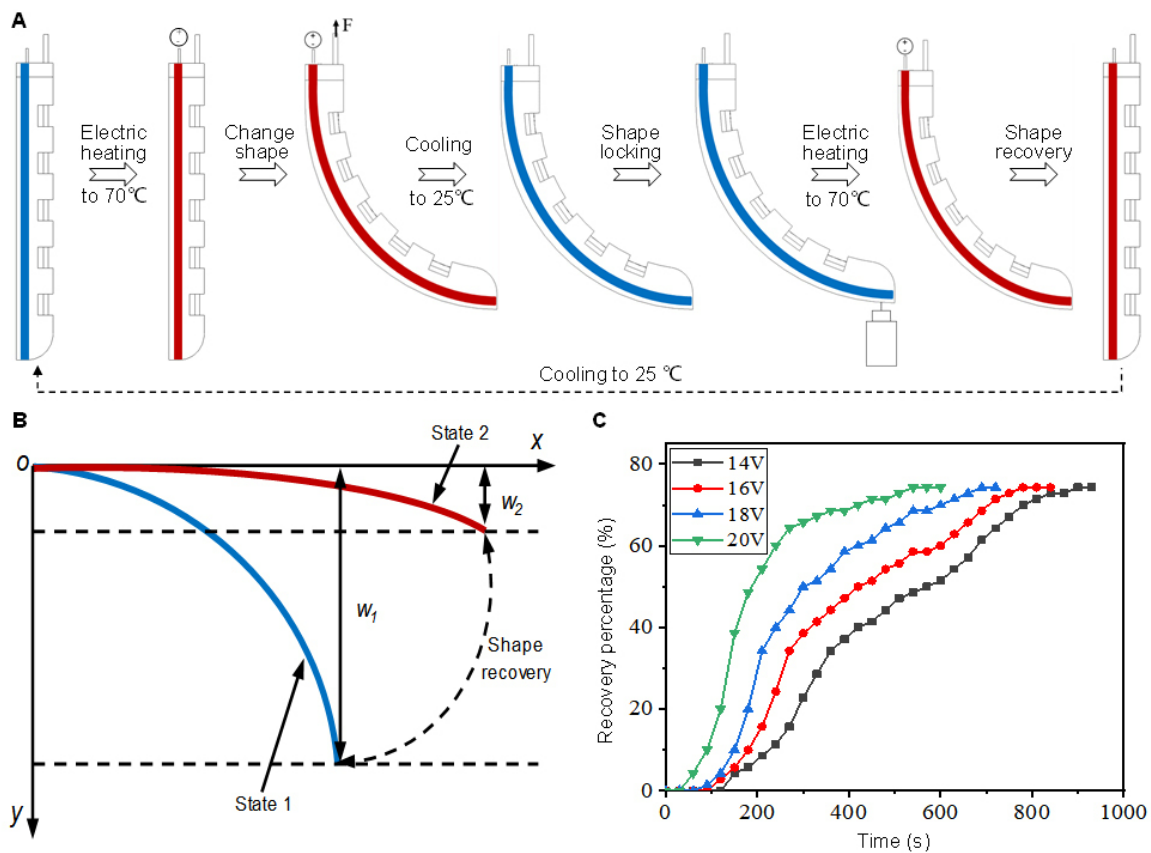
Figure 3. Shape recovery mechanism of Tri-S actuator. (A) Shape recovery process of actuator. (B) Schematic explanation of recovery rate. (C) Characterization of shape recovery under different applied voltages as a function of electrified time.

To observe the dynamic process of temperature, we recorded the temperature distribution image of the Tri-S actuator with heating time under the voltage of 20 V via infrared thermography. Figure 2C illustrates the dynamic temperature states of the Tri-S actuator from 0 to 300 s. The green square with the cross represents the temperature of the central point of the Tri-S actuator. In the first 20 s, the temperature rise is relatively slow, so the temperature of the Tri-S actuator is close to the ambient temperature. After 20 s, the temperature of the Tri-S actuator begins to increase rapidly with increasing time. The color of the Tri-S actuator in the temperature distribution image gradually brightens and is in sharp contrast to the ambient temperature.

The Tri-S actuator also possesses a certain shape recovery function. After the shape is changed under heating conditions, it locks to a temporary shape when cooling to room temperature and also actively restores to the original state by electric heating. Figure 3A illustrates the tunable stiffness process of the actuator. The actuator was first provided Joule heating by a DC power supply. The stiffness of the PLA slice in the Tri-S actuator began to decrease and soften after electric heating. The actuator was actuated to bend by a tendon. The power supply was turned off for a period of time. The temperature of the PLA slice in the actuator was cooled to room temperature. The shape of the actuator could be locked and was able to withstand a certain weight without deformation. When Joule heating was provided again by the DC power

supply, the actuator began to soften and the shape recovered to its initial state.

To observe the recoverability of the Tri-S actuator, we tested the shape recovery percentage under different applied voltages. Figure 3B illustrates the process of the shape recovery of the actuator. In the experiment, the actuator was heated by a DC power supply. A driving force caused the actuator to bend. The terminal displacement (state 1) of the actuator that was created by the driving force is w_1. The driving force was removed after the actuator cooling and shape locking. The actuator was then stimulated by Joule heating. Under the elastic action of TPU, the final displacement (state 2) of the end of the actuator after shape recovery by heating is w_2. The recovery rate is expressed as $\rho = (w_1 - w_2)/w_1$. Figure 3C shows the characterization of recovery rate of the Tri-S actuator as a function of electrified time. The shape recovery percentage of the Tri-S actuator can reach ~75%. Since a certain amount of time was required for the temperature to rise after electric heating, the shape recovery percentage of the Tri-S actuator exhibited no change at the beginning of electrification for each voltage. In contrast, due to the difference in the heating voltage, the starting time point of shape recovery is different. As time goes on, the temperature of the CF heating wire increases and the shape recovery percentage of the Tri-S actuator begins to increase rapidly. The shape recovery percentage increases fastest when the applied voltage is 20 V, which is due to the rapid generation of heat at high voltages. For the applied voltage of 20 V, the recovery rate begins to increase rapidly after 30 s and the growth rate of the recovery rate decreases gradually after 300 s.

Characterization of tunable stiffness and load capacity
By adjusting the electric heating, the stiffness of the actuator can be effectively tuned. Hence, we investigated the relationship between the stiffness of the Tri-S actuator and applied voltage. To measure the stiffness of the Tri-S actuator, a custom-designed experimental platform was set up, as shown in Figure 4A. A fixture was fabricated through the 3D-printing approach. The proximal end of the Tri-S actuator was installed on the fixture and the fixture was fixed on a support frame with the bolts. The weights were hung on the distal end of the Tri-S actuator. A piece of paper with 5 mm-interval grids was adopted to record the deformation of the Tri-S actuator in the experiment.

We conducted dynamic tests of the Tri-S actuator under different applied voltages. In the experiment, the proximal end of the Tri-S actuator was fixed on the support frame via a 3D-printed fixture and a weight of 500 g was hung on the distal end. Four different voltages (14, 16, 18 and 20 V) were applied on both ends of the CF heating wire for heating the Tri-S actuator. In the experiment, we first turned on the power to heat the Tri-S actuator from room temperature (25 °C) to 70 °C by electric heating and then turned off the power to cool naturally from 70 °C to room temperature to investigate the process of its tunable stiffness. Figure 4B shows the process of tunable stiffness. The dotted line represents the boundary between heating and cooling. "H" and "C" represent "heating" and "cooling", respectively. "On" and "Off" represent "turning on" and "turning off" of the heating power supply, respectively. As can be seen, the PLA gradually begins to soften with increasing heating time and the stiffness of the Tri-S actuator decreases for all the applied voltages. The range of obvious stiffness mainly concentrates between 60 and 360 s for the applied voltage of 14 V and the range mainly concentrates between 30 and 150 s for the voltage of 20 V. As depicted in Figure 4B, the higher the applied voltage, the faster the stiffness decrease. The main reason could be that the PLA in the Tri-S actuator will soften faster, owing to increased heat generation for higher voltage and the elasticity of the TPU in the Tri-S actuator being dominant. In particular, for the high voltage (20 V), the stiffness of the Tri-S actuator basically tends to be stable after 180 s. From the experimental results, the stiffness of the actuator can almost return to its original stiffness by the Joule heating effect after the voltage source is switched off.
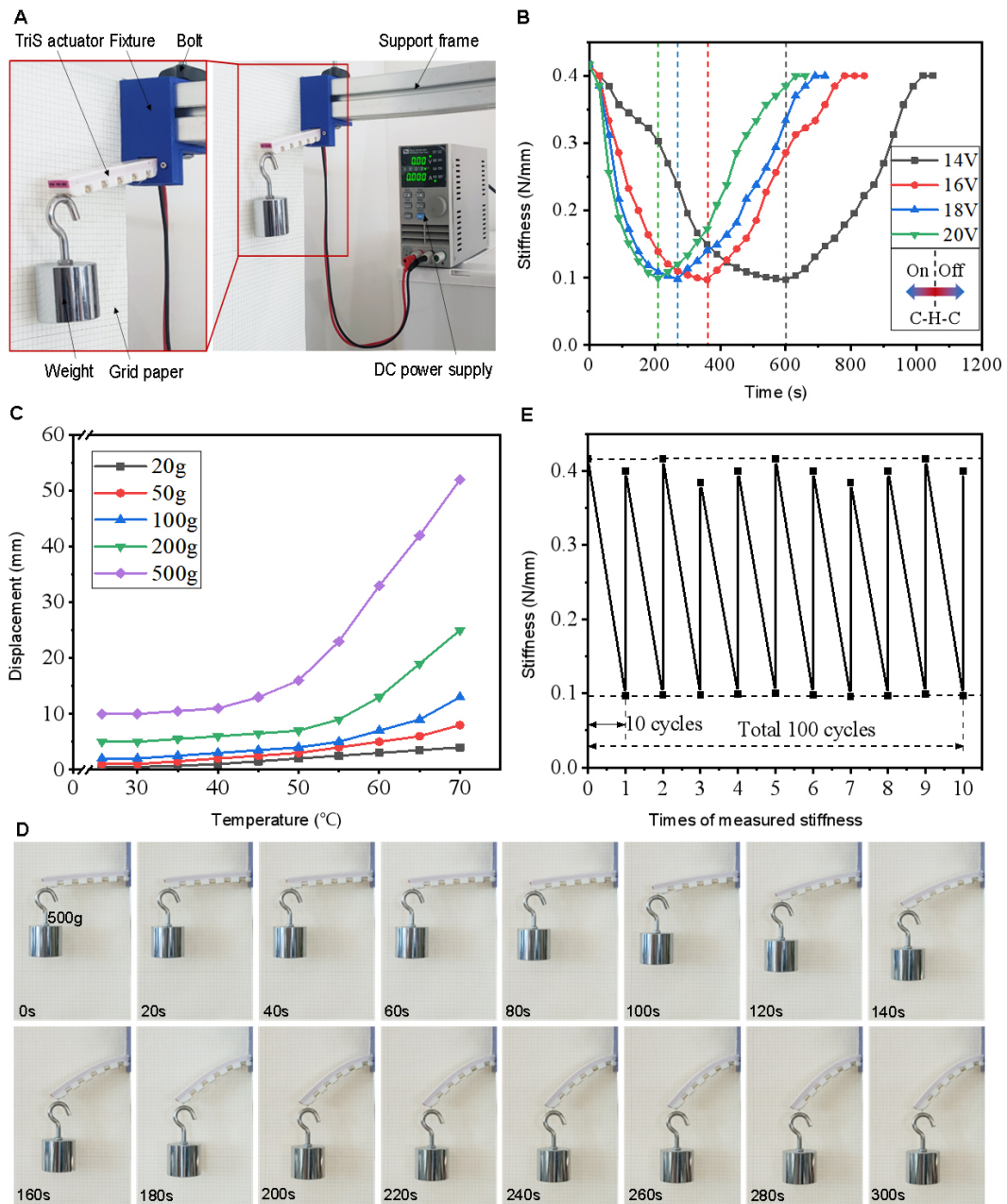
Figure 4. Characterization of tunable stiffness and load capacity of Tri-S actuator. (A) Experimental platform of stiffness test of Tri-S actuator. (B) Stiffness of Tri-S actuator as a function of electrified time. (C) Load capacity characterization of Tri-S actuator with temperature variations. (D) Dynamic variation process of load capacity of Tri-S actuator. (E) Measured stiffness range of actuator after multi-cycle actuation.

To investigate the load capacity, the distal-end displacement of the Tri-S actuator with the temperature (25-70 °C) was measured at five different loads of 20, 50, 100, 200 and 500 g. As shown in Figure 4C, the distal-end displacement of the Tri-S actuator experiences an increase with increasing temperature after heating for all weights. The descent rate of the distal end of the Tri-S actuator progressively increases with increasing weight.

Here, we give an example of the dynamic deformation process of the Tri-S actuator to reflect the stiffness changes over heating time, as shown in Figure 4D. In the experiment, a weight of 500 g was hung on the distal end of the Tri-S actuator. When a voltage of 20 V is applied to the CF heating wire, the PLA in the Tri-S actuator gradually begins to soften with increasing temperature. The stiffness of the Tri-S actuator progressively decreases and the load bearing capacity is weakened accordingly. Therefore, this causes the Tri-S actuator to bend gradually. After 300 s, the degrading displacement of the distal end of the Tri-S actuator reaches 57.5 mm with respect to its initial position.

To validate the durability of PLA in the actuator, we performed a series of multi-cycle actuation tests. Since the heating-cooling process is time-consuming, in order to save time, the experiment was divided into ten sessions and each session contains ten trials. The actuator was heated up to 70 °C and cooled down to room temperature once; we took it as a session and repeated the session ten times. In each session, after the actuator was heated, we actuated the actuator to bend to ~45° and returned to its original position. We took it as a trial and repeated the trial for ten cycles. After each session, we measured the stiffness range of the actuator once. We ran ten sessions in all and the total number of trials was 100 cycles. Figure 4E shows the measured stiffness range after experiencing every ten cycles (trials). From the experimental results, it can be found that the multi-cycle actuation seems to have little effect on the durability of the actuator.

Robotic soft gripper equipped with Tri-S actuators

To further demonstrate the effectiveness of our Tri-S actuator in terms of tunable stiffness and shape locking, we developed a soft robotic gripper using three Tri-S actuators, as shown in Figure 5A. The three Tri-S actuators were installed in a mounting pedestal and the corresponding tendons were fixed in a mounting block. A driving motor was used to actuate the motion of the mounting block by a screw. When the driving motor was running, the tendon was pulled through the mounting block. The Tri-S actuators of the gripper bent and performed a grasp operation under the action of the motor driving force.

Figure 5B and C show the grasping ability of the gripper by modulating the stiffness of the actuators. As can be seen, it cannot only grasp fragile objects (e.g., eggs and apples) without damage due to its inherent softness but can also grasp heavy objects (e.g., metal bars), owing to its high stiffness.

Load capacity tests were performed with an external driving force power supply to validate the tunable stiffness capability of the Tri-S actuator. In the experiment, the power supply was employed to heat the CF heating wire for controlling the stiffness regulation of three Tri-S actuators in the soft robotic gripper. We first turned on the DC power to heat the PLA in the Tri-S actuator. After the PLA was softened, the soft robotic gripper was actuated to grasp objects by pulling the driving tendon under the action of the motor driving force. We then turned off the DC power and naturally cooled the PLA. The objects can be firmly gripped by continually hauling the driving tendon of the gripper. For each object to be grasped, we first conducted pre-grasping tests to estimate the stiffness according to grasping effects before the experiment and then we further performed a formal grasping experiment. On this basis, it could harness the stiffness modulation for better grasping without buckling. As shown in Figure 5B, several objects with different weights (628-2216 g) can be grasped by modulating the stiffness of the Tri-S actuators. We also conducted a grasping test using the actuators without the stiffness-tunable function, which is only able to grasp weights less than 200 g. This indicates that the load capacity of the soft actuators with the stiffness-tunable function can be significantly improved.

To verify the shape-locking ability of the Tri-S actuator, a few holding tests were conducted using the soft robotic gripper. We first turned on the DC power to heat the PLA in the Tri-S actuator. After the PLA was
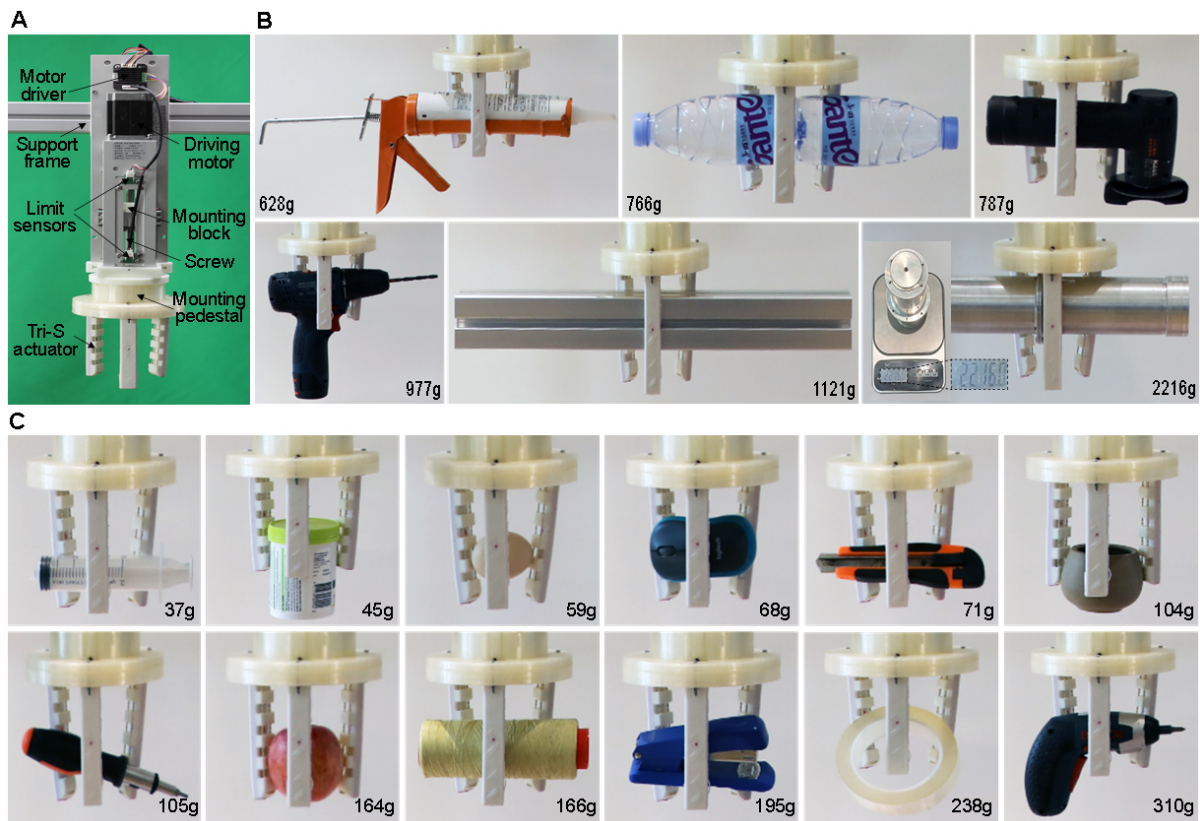
Figure 5. Exhibition of tunable-stiffness and shape-locking capacity of soft gripper. (A) Soft gripper equipped with Tri-S actuators. (B) Loading capacity test of soft gripper. (C) Shape locking capacity test of soft gripper.

softened, we drove the soft robotic gripper to grab objects and lock the grasping state. We then turned off the DC power and naturally cooled the PLA. As shown in Figure 5C, the soft robotic gripper can lock some objects with arbitrary shapes and various weights (from 37 to 310 g) without an external driving source by shape locking by natural cooling. This indicates that our Tri-S actuators have a relatively larger shape-locking function. This can effectively save the energy output of driving power supply during continuously grasping tasks for a long time.

CONCLUSIONS AND FUTURE WORK

We have proposed a novel stiffness-tunable and shape-locking method for soft actuators using 3D-printed hybrid multi-polymer materials manufacturing technology. The easy fabrication of the Tri-S actuator was achieved by the 3D-printing method. The developed Tri-S actuator can not only support heavy loads using its tunable stiffness but can also save the actuating power supply in holding tasks by shape locking. The Tri-S actuator can achieve stiffness modulation and the shape-locking function by conveniently applying electric power at both ends of the CF heating wire to generate Joule heating. The stiffness-tunable and shape-locking capacities are demonstrated by a robotic soft gripper equipped with three assembled Tri-S actuators, which can grasp and lock objects of arbitrary shapes and various weights. In particular, the soft robotic gripper was able to successfully grasp weights up to 2216 g and effectively hold weights up to 310 g without an external driving source by shape locking.

The stiffness of the Tri-S actuator can be effectively tuned by heating. However, there are also some limitations in this work. For example, the cooling time is still a problem to be solved. Effective cooling methods can improve the work efficiency of the Tri-S actuator. In the next step, we plan to explore how to quickly cool down the Tri-S actuator and restore it to the high stiffness state. One possible solution is to use a Peltier for cooling. However, Peltiers are rigid components. To make it flexible, the Peltier can be fabricated into small units and then formed into a Partier array. On this basis, the rigid Peltier can become flexible. Finally, we can install the Partier array on the Tri-S actuator to cool it down. Actually, the proposed stiffness-tunable and shape-locking method is not just limited to the current soft actuator. By adjusting the size and configuration of the tunable stiffness material structure, the method can be used for more types of soft apparatuses or robots, such as pneumatic and hydraulic driven robots, intelligent material driven robots and magnetic driven robots[40-42]. By improving the structure geometry and dimensions of the Tri-S actuator, it could be applied to a variety of soft robots. Through the appropriate control strategy of the stiffness, the soft robots will have both the ability to move flexibly and adapt to high loads.

DECLARATIONS

Authors' contributions
Concept and design: Jiao J, Guo Y, Tong Q, Mei T
Fabrication and method: Jiao J, Guo Y, Liu S
Modeling and analysis: Jiao J, Liu S
Experiment and validation: Jiao J, Liu S, Qiu P
Writing and editing: Jiao J, Guo Y, Tong Q, Liu S, Wang D

Availability of data and materials
Not applicable.

Conflicts of interest
All authors declared that there are no conflicts of interest.

Ethical approval and consent to participate
Not applicable.

Consent for publication
Not applicable.

REFERENCES
1. Renda F, Boyer F, Dias J, Seneviratne L. Discrete cosserat approach for multisection soft manipulator dynamics. *IEEE Trans Robot* 2018;34:1518-33. DOI
2. Yang H, Xu M, Li W, Zhang S. Design and implementation of a soft robotic arm driven by sma coils. *IEEE Trans Ind Electron* 2019;66:6108-16. DOI
3. Singh G, Krishnan G. A constrained maximization formulation to analyze deformation of fiber reinforced elastomeric actuators. *Smart Mater Struct* 2017;26:065024. DOI

4.   Park W, Shin E, Yoo Y, Choi S, Kim S. Soft haptic actuator based on knitted PVC gel fabric. *IEEE Trans Ind Electron* 2020;67:677-85. DOI

5.   Zhao Y, Lo CY, Ruan L, et al. Somatosensory actuator based on stretchable conductive photothermally responsive hydrogel. *Sci Robot* 2021;6:eabd5483. DOI PubMed

6.   Gorissen B, Reynaerts D, Konishi S, Yoshida K, Kim JW, De Volder M. Elastic inflatable actuators for soft robotic applications. *Adv Mater* 2017;29:1604977. DOI PubMed

7.   Zhang J, Zhao J, Wang S, Chen H, Li D. Large stable deformation of dielectric elastomers driven on mode of steady electric field. *Smart Mater Struct* 2017;26:05LT01. DOI

8.   Shintake J, Cacucciolo V, Floreano D, Shea H. Soft robotic grippers. *Adv Mater* 2018:e1707035. DOI PubMed

9.   Chen S, Pang Y, Cao Y, Tan X, Cao C. Soft robotic manipulation system capable of stiffness variation and dexterous operation for safe human-machine interactions. *Adv Mater Technol* 2021;6:2100084. DOI

10. Manti M, Hassan T, Passetti G, D'elia N, Laschi C, Cianchetti M. A bioinspired soft robotic gripper for adaptable and effective grasping. *Soft Robot* 2015;2:107-16. DOI

11. Shapiro Y, Wolf A, Gabor K. Bi-bellows: pneumatic bending actuator. *Sens Actuators A Phys* 2011;167:484-94. DOI

12. Henke M, Sorber J, Gerlach G. Multi-layer beam with variable stiffness based on electroactive polymers. In proceedings of spie-the international society for optical engineering. 2012. pp. 83401P-13. DOI

13. Choi I, Corson N, Peiros L, Hawkes EW, Keller S, Follmer S. A soft, controllable, high force density linear brake utilizing layer jamming. *IEEE Robot Autom Lett* 2018;3:450-7. DOI

14. Zhu M, Do TN, Hawkes E, Visell Y. Fluidic fabric muscle sheets for wearable and soft robotics. *Soft Robot* 2020;7:179-97. DOI PubMed

15. Liu S, Jiao J, Meng F, Mei T, Sun X, Kong W. Modelling of a soft actuator with a semicircular cross section under gravity and external load. *IEEE Trans Ind Electron* 2022;5:4952-61. DOI

16. Liu S, Jiao J, Kong W, et al. Modeling of a bio-inspired soft arm with semicircular cross section for underwater grasping. *Smart Mater Struct* 2021;30:125029. DOI

17. Wang Z, Wang D, Zhang Y, et al. A three-fingered force feedback glove using fiber-reinforced soft bending actuators. *IEEE Trans Ind Electron* 2020;67:7681-90. DOI

18. Manti M, Cacucciolo V, Cianchetti M. Stiffening in soft robotics: a review of the state of the art. *IEEE Robot Automat Mag* 2016;23:93-106. DOI

19. Jiang A, Ranzani T, Gerboni G, et al. Robotic granular jamming: does the membrane matter? *Soft Robot* 2014;1:192-201. DOI

20. Majidi C, Wood RJ. Tunable elastic stiffness with microconfined magnetorheological domains at low magnetic field. *Appl Phys Lett* 2010;97:164104. DOI

21. Jiang P, Yang Y, Chen MZQ, Chen Y. A variable stiffness gripper based on differential drive particle jamming. *Bioinspir Biomim* 2019;14:036009. DOI PubMed

22. Jiang A, Xynogalas G, Dasgupta P, Althoefer K, Nanayakkara T. Design of a variable stiffness flexible manipulator with composite granular jamming and membrane coupling. In proceedings of 2012 IEEE/RSJ international conference on intelligent robots and systems. 2012. pp. 2922-27. DOI

23. Taghavi M, Helps T, Huang B, Rossiter J. 3D-printed ready-to-use variable-stiffness structures. *IEEE Robot Autom Lett* 2018;3:2402-7. DOI

24. Ze Q, Kuang X, Wu S, et al. Magnetic shape memory polymers with integrated multifunctional shape manipulation. *Adv Mater* 2020;32:e1906657. DOI PubMed

25. Nakagawa M, Luding S, Pournin L, Tsukahara M, Liebling TM. Particle shape versus friction in granular jamming. In proceedings of AIP Conference Proceedings. 2009. Volume 1145, pp. 499-502. DOI

26. Amend JR, Brown E, Rodenberg N, Jaeger HM, Lipson H. A positive pressure universal gripper based on the jamming of granular material. *IEEE Trans Robot* 2012;28:341-50. DOI

27. Kim YJ, Cheng S, Kim S, Iagnemma K. Design of a tubular snake-like manipulator with stiffening capability by layer jamming. In proceedings of 2012 IEEE/RSJ international conference on intelligent robots and systems. 2012. pp. 4251-6. DOI

28. Li Y, Chen Y, Yang Y, Wei Y. Passive particle jamming and its stiffening of soft robotic grippers. *IEEE Trans Robot* 2017;33:446-55. DOI

29. Kim Y, Cheng S, Kim S, Iagnemma K. A novel layer jamming mechanism with tunable stiffness capability for minimally invasive surgery. *IEEE Trans Robot* 2013;29:1031-42. DOI

30. Jiang Y, Chen D, Liu C, Li J. Chain-like granular jamming: a novel stiffness-programmable mechanism for soft robotics. *Soft Robot* 2019;6:118-32. DOI PubMed

31. Xie T. Tunable polymer multi-shape memory effect. *Nature* 2010;464:267-70. DOI PubMed

32. Yuen MC, Bilodeau RA, Kramer RK. Active variable stiffness fibers for multifunctional robotic fabrics. *IEEE Robot Autom Lett* 2016;1:708-15. DOI

33. Hao Y, Wang T, Xie Z, et al. A eutectic-alloy-infused soft actuator with sensing, tunable degrees of freedom, and stiffness properties. *J Micromech Microeng* 2018;28:024004. DOI

34. Xu W, Huan AS, Ren H. Prototyping and characterisation of a variable stiffness actuation mechanism based on low melting point polymer. *Int J Mechatron Autom* 2016;5:211. DOI

35.   Shintake J, Schubert B, Rosset S, Shea H, Floreano D. Variable stiffness actuator for soft robotics using dielectric elastomer and low-melting-point alloy. In proceedings of 2015 IEEE/RSJ international conference on intelligent robots and systems (IROS). 2015. pp. 1097-102. DOI

36.   Hao Y, Wang T, Xi F, Kang Y, Li W. A variable stiffness soft robotic gripper with low-melting-point alloy. In proceedings of 2017 36th Chinese Control Conference (CCC). 2017. pp. 6781-6. DOI

37.   Zhang Y, Zhang N, Hingorani H, et al. Soft robots: fast-response, stiffness-tunable soft actuator by hybrid multimaterial 3D printing. *Adv Funct Mater* 2019;29:1970098. DOI

38.   Schubert BE, Floreano D. Variable stiffness material based on rigid low-melting-point-alloy microstructures embedded in soft poly(dimethylsiloxane) (PDMS). *RSC Adv* 2013;3:24671. DOI

39.   Al-Rubaiai M, Pinto T, Qian C, Tan X. Soft actuators with stiffness and shape modulation using 3D-printed conductive polylactic acid material. *Soft Robot* 2019;6:318-32. DOI PubMed

40.   Li Y, Chen Y, Ren T, Li Y, Choi SH. Precharged pneumatic soft actuators and their applications to untethered soft robots. *Soft Robot* 2018;5:567-75. DOI

41.   He Q, Wang Z, Wang Y, Minori A, Tolley MT, Cai S. Electrically controlled liquid crystal elastomer-based soft tubular actuator with multimodal actuation. *Sci Adv* 2019;5:eaax5746. DOI PubMed PMC

42.   Alcântara CCJ, Kim S, Lee S, et al. 3D fabrication of fully iron magnetic microrobots. *Small* 2019;15:e1805006. DOI PubMed